ACS APPLIED MATERIALS & INTERFACES

Research Article

www.acsami.org

Graphene Oxide–$MnFe_2O_4$ Magnetic Nanohybrids for Efficient Removal of Lead and Arsenic from Water

Suresh Kumar,[†] Rahul R. Nair,[‡] Premlal B. Pillai,[§] Satyendra Nath Gupta,[†] M. A. R. Iyengar,[†] and A. K. Sood*[,†]

[†]Department of Physics, Indian Institute of Science, Bangalore 560012, India

[‡]School of Physics and Astronomy, University of Manchester, Manchester M13 9PL, U.K.

[§]Department of Electronic and Electrical Engineering, University of Sheffield, Sheffield S1 3JD, U.K.

Supporting Information

ABSTRACT: We show that the hybrids of single-layer graphene oxide with manganese ferrite magnetic nanoparticles have the best adsorption properties for efficient removal of Pb(II), As(III), and As(V) from contaminated water. The nanohybrids prepared by coprecipitation technique were characterized using atomic force and scanning electron microscopies, Fourier transformed infrared spectroscopy, Raman spectroscopy, X-ray diffraction, and surface area measurements. Magnetic character of the nanohybrids was ascertained by a vibrating sample magnetometer. Batch experiments were carried out to quantify the adsorption kinetics and adsorption capacities of the nanohybrids and compared with the bare nanoparticles of $MnFe_2O_4$. The adsorption data from our experiments fit the Langmuir isotherm, yielding the maximum adsorption capacity higher than the reported values so far. Temperature-dependent adsorption studies have been done to estimate the free energy and enthalpy of adsorption. Reusability, ease of magnetic separation, high removal efficiency, high surface area, and fast kinetics make these nanohybrids very attractive candidates for low-cost adsorbents for the effective coremoval of heavy metals from contaminated water.

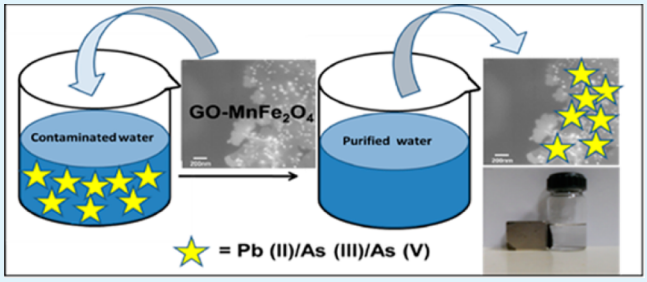

KEYWORDS: *graphene, magnetic nanohybrids, adsorption kinetics, absorbents, heavy metals, water treatment*

1. INTRODUCTION

Rapidly growing industrialization and urbanization have increased the concentration of various toxic heavy metals like As, Pb, Cd, and Hg in natural potable waters beyond acceptable tolerance limits. The exposure to these heavy metals is considered a major health risk due to their toxic and carcinogenic effects.[1] Arsenic due to its high toxicity and carcinogenicity has caused severe health problems worldwide.[1] Arsenic is a metalloid commonly occurring in two most common valence states: arsenate (As(V)) and arsenite (As(III)) under oxidized forms. The former is more common in aerobic surface water whereas the latter is more abundant in anaerobic groundwater. The effects of arsenic poisoning are most severe in India and Bangladesh,[2,3] where concentration can range from 0.05 to 0.3 mg/L and in isolated cases registered a concentration of up to 3 mg/L.[4] The permissible level of arsenic in groundwater is up to10 μg/L.[5]

Another common groundwater contaminant which is extremely detrimental to human health is lead (Pb(II)). The toxicity comes from its ability to mimic other biologically important metals, the most notable of which are calcium, iron, and zinc. Lead builds up in the body over the years and can cause damage to the brain, red blood cells, and kidneys.[6,7]

A clear realization that the world faces major threats to community health from its water supplies in the form of contamination has motivated many studies to develop nanomaterials for water purification.[6,8] These functional materials include redox and catalytically active nanoparticles, nanostructured membranes, and bioactive nanoparticles. In recent years, magnetic nanoparticles of Fe_3O_4 have been used to remove arsenic from water.[9] Magnetic nanoparticles are useful because of their key properties such as magnetic separation and ease to functionalize with various chemical groups to increase their affinity toward target compounds and high surface-to-volume ratio.[10] Organic matter and heavy-metal reducing capabilities of zerovalent iron,[11] titanium oxide,[12] zeolites,[13] and ZnO[14] have been identified. Lead-removing capabilities of carbon aerogels,[15] Mn–diatomite,[16] activated carbon,[17] polymer-supported zirconium phosphate,[18] and mixture of manganese (hydro) oxides and iron (hydro) oxides[19] have been shown.

The toxicity and solubility of As(III) is relatively greater than As(V).[1] Numerous reports are available describing the action of

Received: March 11, 2014
Accepted: September 15, 2014
Published: September 15, 2014

   dx.doi.org/10.1021/am504826q | ACS Appl. Mater. Interfaces 2014, 6, 17426–17436

manganese oxides for the oxidation of As(III) to As(V).[20−24] The oxidation rate of As(III) in the presence of Fe(III) complexes is suggested to be significantly lower than those in the presence of Mn(IV) complexes.[25] Magnetite,[26] natural Fe−Mn-enriched samples[27] and Fe−Mn binary oxide,[28] have been proven to be promising arsenic adsorbents. The summary of these results are given in Table 1. The potential of $MnFe_2O_4$ nanoparticles for the effective removal of Cr(VI),[29] Azo dye acid Red B (ARB),[30] and arsenic[31] have been recently reported.

Table 1. Adsorption Results Using Various Adsorbents

	adsorbent	adsorption capacity (mg/g)	reference
Pb(II)	chitosan/graphene oxide composites	76.9	62
	GO	328	7
	EDTA−GO	479	7
	EDTA−RGO	204	7
	amino-functionalized carbon nanotubes	58.3	63
	chitosan/alginate composite beads	60.3	64
	graphene nanosheets	35.5	65
	few layered GO	842 (293 K)	68
	few layered GO	1150 (313 K)	68
	few layered GO	1850 (333 K)	68
	GO/chitosan	99	69
	GO−gelatin/chitosan	100	70
	$MnFe_2O_4$ nanoparticles	**488**	**present work**
	GO−$MnFe_2O_4$ nanohybrids	**673**	**present work**
As(III)	magnetite (11.72 nm)	114.7	26
	magnetite (20 nm)	29.1	26
	magnetite (300 nm)	1.6	26
	Fe−Mn mineral material	12	27
	Fe−Mn composite	132.6	28
	functionalized graphene	138.8	3
	functionalized MWCNTs	109.5	67
	MWNT/Fe_3O_4 hybrid	39	66
	$MnFe_2O_4$ nanoparticles	**97**	**present work**
	GO−$MnFe_2O_4$ nanohybrids	**146**	**present work**
As(V)	Fe−Mn composite	69.7	28
	Fe−Mn mineral material	6.7	27
	magnetite (300 nm)	1.1	26
	magnetite (20 nm)	11.4	26
	magnetite (11.72 nm)	46.5	26
	functionalized graphene	142	3
	MWNT/Fe_3O_4 hybrid	53	66
	$MnFe_2O_4$ nanoparticles	**136**	**present work**
	GO−$MnFe_2O_4$nanohybrid	**207**	**present work**

On the other hand, graphene, a single-atom thick graphitic layer, has interesting physio-chemical properties. Recently, heavy-metal adsorption on graphene-based materials has been demonstrated with good adsorption properties.[7,32,33] Graphene oxide (GO) is particularly an interesting graphene-based material because of its easy production and bulk availability. Graphene oxide has a large number of oxygenated functionalities and high surface area, making it useful for environmental and biological applications.[34,35] Even though GO is a good adsorbent for many ions,[31,32] its efficient removal from water after the treatment is still challenging. To overcome this issue, we have synthesized magnetic $MnFe_2O_4$ nanoparticles (NP) and GO−$MnFe_2O_4$ hybrid (GONH) and investigated their use for coremoval of As and Pb contamination from water. GONH was synthesized using coprecipitation technique and characterized by atomic force microscopy (AFM), Raman spectroscopy, Fourier transform infrared (FTIR) spectroscopy, X-ray photoelectron spectroscopy, scanning electron microscopy (SEM), and X-ray diffraction. Magnetic properties of GONH were quantified using a vibrating sample magnetometer. Inductively coupled plasma atomic emission spectroscopy was used to study the adsorption capacity and kinetics of NP, GO, and GONH for Pb(II), As(V), and As(III) ions.

2. EXPERIMENTAL DETAILS: SYNTHESIS AND CHARACTERIZATION

2.1. Synthesis and Characterization of Graphene Oxide. Graphene oxide was prepared from graphite using a previously reported method with slight modification.[36,37] Briefly, 3 g of graphite flakes were dissolved in H_2SO_4:H_3PO_4 (360:40 mL) acid mixture and 18g of $KMnO_4$ was added slowly under continuous stirring conditions. The temperature of the reaction mixture was increased to 50 °C and continuously stirred for 12 h. Afterward, the suspension was cooled to room temperature and mixed with ∼400 mL ice water containing 3 mL of 30% H_2O_2 followed by sonication for half an hour to exfoliate GO into single layers. The diluted mixture was then centrifuged for 15 min at 10 000 rpm. The solid residue was washed with 30% HCl followed by multiple washings with water and then vacuum-dried at room temperature for 12 h. The average flake size as measured by SEM and AFM is ∼2 μm. The average thickness of the GO flake measured using AFM (Bruker Veeco Innova) is ∼1 nm as shown in Figure 1a, consistent with previous reports.[36,37] X-ray powder diffraction patterns of GO were recorded using Cu Kα radiation (λ = 1.542 Å) (Philips X'Pert Pro). Figure 2a gives the XRD pattern of GO showing a diffraction peak at scattering angle 2θ = 9.4° corresponding to (001) plane of GO, giving the interlayer separation to be ∼9.5 Å. Raman spectra were recorded using LABRAM HR-800 equipped with a 514 nm laser. Raman spectrum of GO in Figure 3a shows two prominent peaks at 1590 and 1342 cm^{-1} related to first-order E_{2g} mode from sp^2 carbon domains (G-band) and disorder mode (D-band),[38] respectively. FTIR spectrum of GO shown in Figure 4a reveals characteristic absorption peaks at 1729, 1620, 1415, 1046, and 1236 cm^{-1}, which can be attributed to C═O stretching or C═C in-plane stretching vibrations or due to adsorbed water molecules, O−H deformation, alkoxy C−O stretching, and epoxy C−O stretching vibrations, respectively.[39,40] All these results clearly indicate the formation of graphene oxide and presence of oxygenated functionalities on a graphene skeleton, which we have used for the growth of magnetic nanoparticles. The −OH and −COOH groups on its surface can have different charge depending upon the pH of the solution.

2.2. Synthesis and Characterization of $MnFe_2O_4$ Nanoparticles. Reference nanoparticles of $MnFe_2O_4$ were synthesized according to a previously reported method.[41] Briefly, 2.7 g of $FeCl_3 \cdot 6H_2O$ and 0.845 g of $MnSO_4 \cdot H_2O$ were dissolved in 100 mL of deionized water so that the molar ratio of Mn:Fe in the solution is 1:2. The solution was then constantly stirred and heated to 80 °C. To this, 8 M NaOH heated to the same temperature was added slowly (under continuous stirring) to raise the pH of the solution to 10.5. The reaction was continued for 5 min and then cooled down to room temperature. The blackish precipitates were magnetically separated and washed with excess of water to remove the unreacted content followed by washing with acetone. Afterward, the precipitates were dried at room temperature for 24 h. Figure 2b shows the X-ray diffraction pattern from the NP. The average particle size calculated using Debye−Scherrer equation $D = K\lambda/\beta \cos \theta$ (K is a constant having value 0.9 and β is the full-width at half-maximum of the

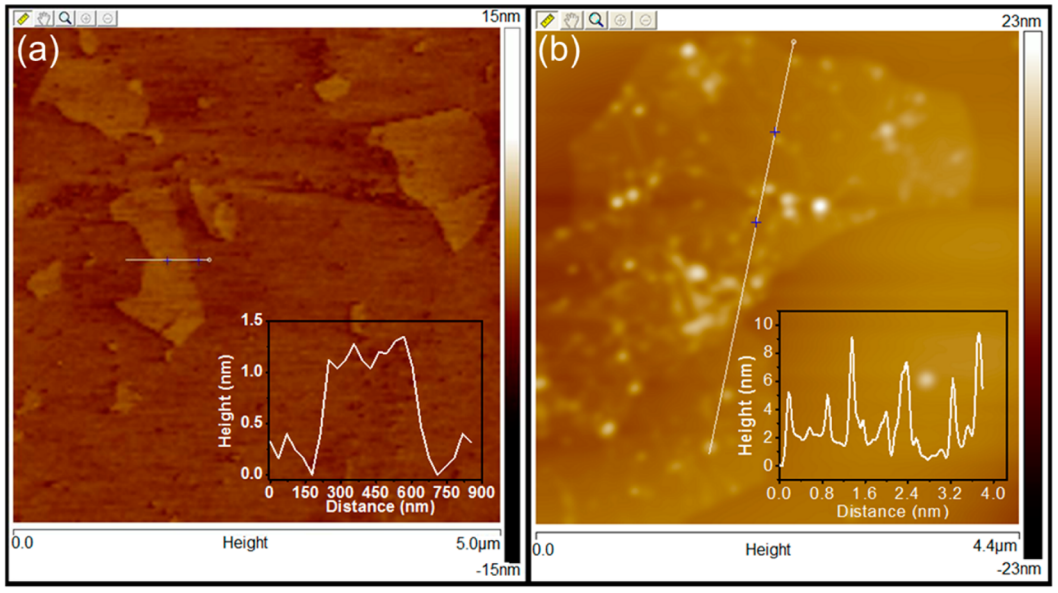

Figure 1. Atomic force microscopic image of GO (a) and GONH (b).

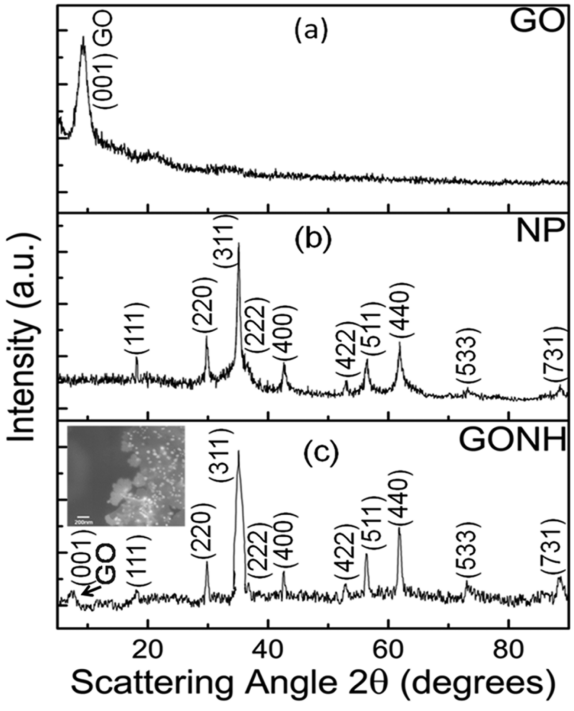

Figure 2. XRD pattern of graphene oxide (a), NP (b), GONH (c), and typical FESEM image of GONH (inset of (c)).

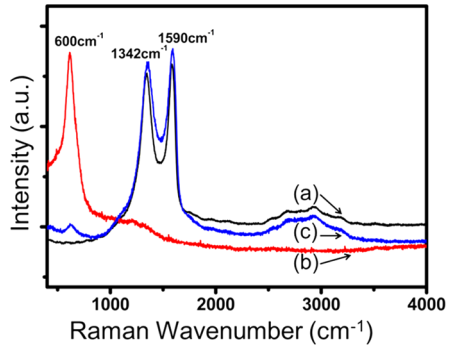

Figure 3. Raman spectra of GO (a), NP (b), and GONH (c).

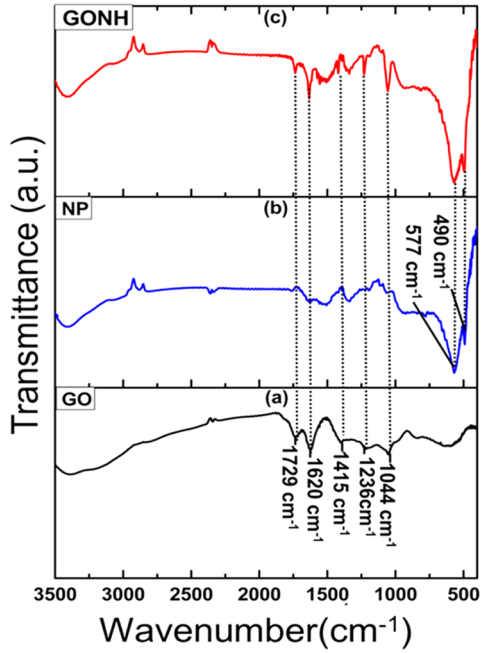

Figure 4. FTIR spectra of GO (a), NP (b), and GONH (c).

diffraction peak) is ~11 nm (considering (311) line). This is close to the height of the nanoparticle (8 nm) measured using atomic force microscope. Raman spectrum of the NPs (Figure 3b) shows a peak at ~600 cm^{-1}, which can be attributed to Fe−O bond stretching.[42] FTIR spectrum of NP (Figure 4b) exhibits absorption peaks at 490 and 577 cm^{-1} due to metal−O stretching vibrations of manganese ferrite.[43] FTIR and Raman results confirm the formation of $MnFe_2O_4$ nanoparticles

Magnetic behavior of these nanoparticles was analyzed using Quantum Design PPMS (Physical Property Measurement System) and is shown in Figure 5. The magnetization was measured as a function of temperature in the presence of an applied field of 250 Oe in field-cooled (FC) and zero-field-cooled (ZFC) conditions between 5 and 300 K temperatures. The observed temperature dependence

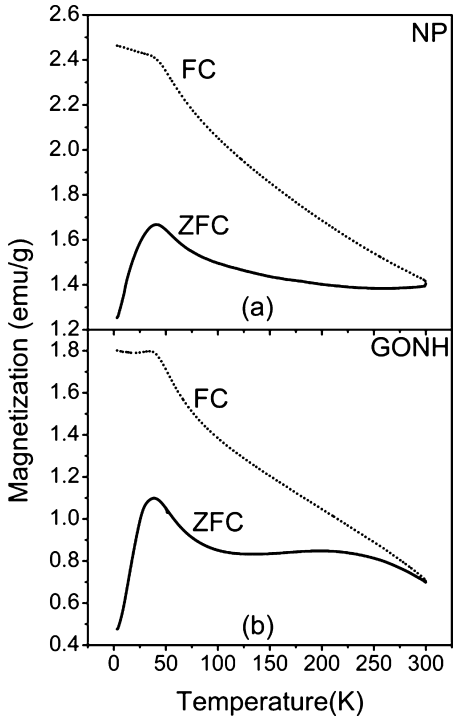

Figure 5. FC−ZFC curves for NP (a) and GONH (b).

agrees with the reported room-temperature superparamagnetic behavior of $MnFe_2O_4$ nanoparticles.[44] The field dependence of magnetization (M−H measurement) of the nanoparticles is given in Figure 6a at 5 and 300 K. The results confirm the high magnetization value of the nanoparticles. The magnetic behavior of these nanoparticles is helpful in easy magnetic separation of the nanoparticles after the completion of the adsorption process.

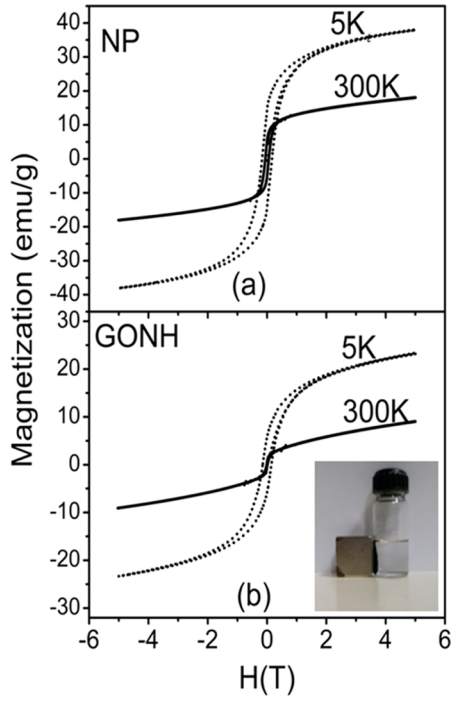

Figure 6. Hysteresis (M−H) curves for NP (a) and GONH (b) at 5 and 300 K and digital camera image of magnetic separation of GONH with small magnet.

2.3. Synthesis and Characterization of GO−$MnFe_2O_4$ Nanohybrids. Graphene oxide (0.5 g) was added to 400 mL of water and dispersed by ultrasonication for 5 min. In turn, 2.7 g of $FeCl_3{\cdot}6H_2O$ and 0.845 g of $MnSO_4{\cdot}H_2O$ were added to the colloidal graphene oxide solution and stirred for half an hour. The temperature of the solution was raised to 80 °C under continuous stirring conditions. Afterward, the pH of this solution was raised to 10.5 by addition of 8 M NaOH (heated to the same temperature). The reaction was continued for 5 min and then cooled to room temperature. The nanohybrid particles were magnetically separated and washed with excess of water and acetone. The precipitates were then dried at room temperature for 24 h. Figure 2c represents the X-ray diffraction pattern of the GONH exhibiting diffraction peaks of both the NP and the GO flakes. The average size of the NP grown on the surface of graphene oxide is ∼6 nm as measured by AFM (shown in Figure 1b). In Figure 2c, the peak due to the (001) reflection plane of GO is decreased due to partial reduction of graphene oxide during the synthesis of the nanohybrids. The peaks corresponding to α-Fe_2O_3 and α-MnO_2 on the surface of the particles in the XRD pattern are absent, indicating the formation of NP and GONH. The average size of the nanoparticles through XRD analysis is ∼7.5 nm. In the XRD pattern of the nanohybrids, the peak of GO is very much diminished due to the fact that the nanoparticles grown on the surface of graphene oxide avert its restacking.[45] The decrease in the size of the nanoparticles in nanohybrid may be attributed to the fact that one side of the nanoparticles growth was blocked when grown in situ onto the surface of the graphene. Raman spectrum of the GONH given in Figure 3c shows the Raman lines of NPs as well as that of GO. Similarly, the FTIR (Thermo-Nicolet 6700) spectrum of the GONH (Figure 4c) exhibits the characteristic peaks of GO and NP. These results indicate that the nanohybrids have been prepared successfully. The typical scanning electron micrograph of the nanohybrid is shown in the inset of Figure 2c. The coverage of the nanoparticles on graphene was found to be uniform for different samples. The FC and ZFC plots of GONH (Figure 5) show superparamagnetic behavior of GONH particles and their behavior is qualitatively similar to that of the pristine NP. The M−H measurements of the nanohybrids are given in Figure 6b at 5 and 300 K. XPS analysis (Axis Ultra) of the hybrids is given in Figure7a. The C(1s) spectrum of the nanohybrids shows peaks at 284.6, 286.7, and 288.4 eV associated with sp^2 C−C, C−O, and C═O bonds, repectively.[46] In the O(1s) spectrum (Figure 7b), the peaks at 529.5, 530.8, and 531.8 eV are due to the presence of O^{2-}, O−H bond,

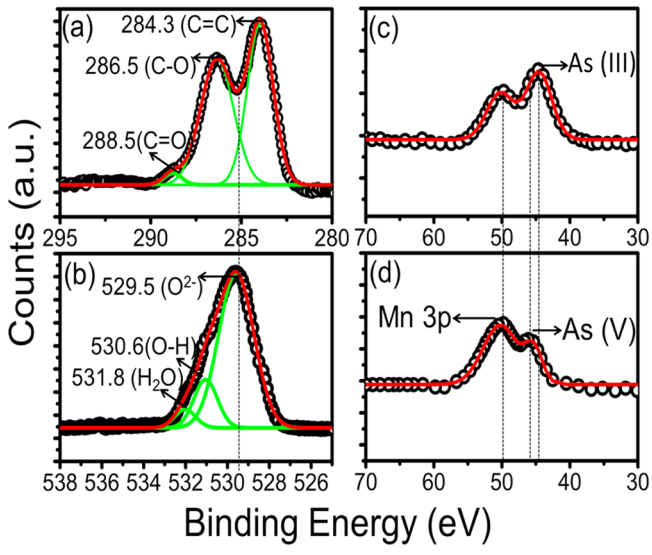

Figure 7. XPS spectra of GONH: C(1s) showing peaks of GO (a), O(1s) showing peaks of $MnFe_2O_4$ (b), As(3d) showing conversion of As(III) to As(V) after 10 min adsorption, (c) and after 2 h of adsorption (d).

and adsorbed H_2O, respectively.[47] As the 3d spectra of As(III) adsorbed GONH after 10 min and 4 h, adsorption reaction times are shown in parts (c) and (d), respectively, of Figure 7. The surface area measurements of the NP and GONH were carried out using the Brunauer, Emmet, and Teller (BET) method (Micromeritics surface area analyzer ASAP 2020) for N_2 gas adsorption. BET surface area for GONH was 196 m^2/g compared to 91 m^2/g for NP. The high surface area favors the high adsorption capacity of these adsorbents.

2.4. Arsenic and Lead Solutions. Analytical grade As(III) oxide (As_2O_3), As(V) oxide (As_2O_5), and lead(II) nitrate ($Pb(NO_3)_2$) were used to prepare stock solutions of 400 mg/L As(III), As(V), and Pb(II), respectively. As_2O_3 and As_2O_5 chemicals were procured from Rolex Chemical Industries, India, and $Pb(NO_3)_2$ was procured from SD Fine Chem Ltd., India. The Secondary As and Pb standards ranging from 1 to 400 mg/L were prepared from the respective stock solutions for the generation of the calibration curves for As and Pb detection. The heavy-metal concentrations were quantitatively measured with the help of an inductively coupled plasma atomic emission spectrometer (Thermo-iCAP 6000 Series) in accordance with the standard method.[48]

2.5. Adsorption Studies. Batch experiments were carried out to understand the adsorption behavior and study the kinetics of heavy-metal adsorption. In separate experiments, 200 mg/L (0.02 wt %) NP and GONH were added to the heavy-metal solutions of varying concentrations ranging from 1 to 400 mg/L made up from stock solution using 0.01 M $NaNO_3$ solution as background electrolyte to keep the ionic strength optimum for adsorption.[49] McBridge[50] suggested that the dominant surface interaction between adsorbate ion forming outer sphere complexation with an adsorbent surface shows decreasing adsorption with increasing ionic strength of the solution.[29] For understanding the adsorption behavior of the nanoparticles and nanohybrids, heavy-metal solutions of varying concentration were sonicated for 10 min and equilibrated for 20 h. The adsorption behavior of the nanoparticles was investigated at different pH values of the heavy-metal solution under study. The solution pH was adjusted by using 1 M NaOH and 1 M HNO_3 as required. For kinetic studies, the pH was fixed at a value corresponding to maximum adsorption and 0.02 wt % of NP and GONH were used. In addition, 0.2 wt % of NP and GONH were also used for adsorption of As(III) and As(V). The initial concentration of the heavy metal was fixed at 20 mg/L and adsorption time was varied from 1 to 120 min. The adsorption isotherm was tested to validate the heavy-metal uptake behavior of the nanoparticles. All samples were analyzed after removing the GONH/NP from the sample by using a small magnet as shown in the inset of Figure 6b. Adsorption behavior was studied at 298, 313, and 333 K to understand the thermodynamics of the adsorption process.

2.6. Effect of Competing Ions. In the contaminated water there exist many common ions (both cations and anions) which affect the adsorption of a particular metal ion (in our case, metal ions are (Pb(II), As(III), and As(V)). These ions compete to bind to the adsorbent surface, affecting the adsorption of a particular heavy-metal ion. Therefore, it is important to study their role during the adsorption process. We have studied the effect of NO^{3-}, SO_4^{2-}, HCO_3^-, HPO_4^{2-}, Cd^{2+}, and Zn^{2+}ions on the adsorption of arsenic and lead ions on GONH and NP adsorbents with varied concentrations of the competing ions.

2.7. Desorption Studies and Regeneration. High adsorption capacity and better desorption capability of an adsorbent are the two important factors which impact their application. The pH of water affects the adsorption and desorption capabilities of adsorbent. At high pH conditions, the surface functional groups become negatively charged due to deprotonation of the surface functional groups (−OH and −COOH) and therefore the adsorbed arsenic species are desorbed.[31] Therefore, desorption of arsenic ions is conducted by treatment with 1 M NaOH (2 mL). Contrary to this, Pb(II) ions are desorbed at low pH values (due to protonation of the surface functional groups), and therefore, desorption in this case was conducted through treatment with 0.2 M HCl.

3. RESULTS AND DISCUSSION

Aqueous solutions of metal ions, Pb(II), As(III), and As(V) with different concentrations were treated with NP and GONH. The amount of the ionic metal adsorbed on nanoparticles and hybrids is calculated using the relation $q_e = ((C_0 - C_e)/m)V$. Here, q_e (mg/g) is the amount of metal ions adsorbed by the adsorbent at equilibrium condition, C_0 is the initial metal ion concentration, C_e is the metal ion concentration at equilibrium, V is the volume of the ionic solution, and m is the mass of the adsorbent. On the basis of assumptions such as uniform surface single layer of adsorbent material, the Langmuir isotherm between quantities adsorbed at equilibrium q_e and initial equilibrium concentration (C_e) can be expressed as

$$q_e = \frac{bC_e q_m}{1 + bC_e} \quad (1)$$

where b is the Langmuir constant. The parameter q_m is the maximum concentration of the adsorbed quantity of the heavy metals. Equation 1 can be written in linearized form as

$$\frac{C_e}{q_e} = \frac{C_e}{q_m} + \frac{1}{q_m} \quad (2)$$

The percentage removal of heavy metals being plotted is $100(C_0 - C_e)/C_0$.

3.1. Effect of pH of the Solution. The pH of the solution is found to be an important factor to affect the degree of surface charge ionization and speciation of the adsorbate. The adsorption data of NP and GONH in the case of Pb(II), As(V), and As(III) at different pH conditions are shown in parts (a), (b), and (c), respectively, of Figure 8, with initial concentration of 100 mg/L. The maximum adsorption occurs at pH = 5 for Pb(II), pH = 4 for As(V) and pH = 6.5 for As(III). There is a slight change in initial and final pH values. The values of initial and final pH values are given in Table 2.

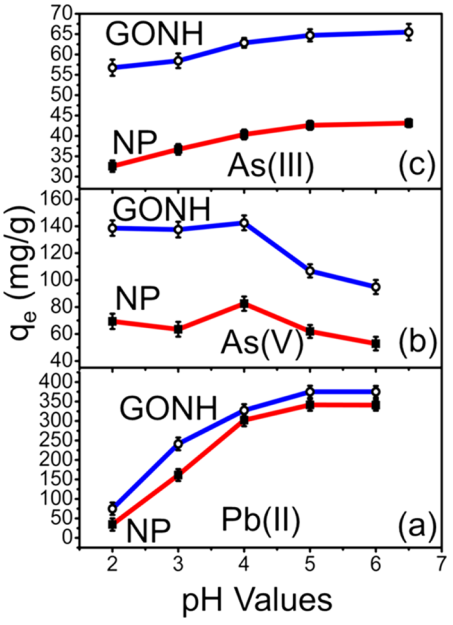

Figure 8. Adsorption of the metal ions Pb(II) (a), As(V) (b), and As(III) (c) at different pH values with initial concentration of 100 mg/L.

Table 2. Initial (before Adsorption) and Final (after Adsorption) pH Values

		initial pH					final pH				
heavy-metal ion	adsorbent										
Pb(II)	NP	2	3	4	5	6	1.9	2.87	3.85	4.55	5.6
	GONH	2	3	4	5	6	1.88	2.85	3.83	4.5	5.48
As(V)	NP	2	3	4	5	6	2.25	3.34	4.41	5.42	6.8
	GONH	2	3	4	5	6	2.27	3.38	4.38	5.46	6.85
As(III)	NP	2	3	4	5	6.5	2.2	3.31	4.35	5.25	6.75
	GONH	2	3	4	5	6.5	2.18	3.29	4.4	5.2	6.72

3.2. Langmuir Isotherms and Adsorption Capacities. After finding the optimum pH, adsorption of different concentrations of metal ions were investigated and the data were fitted to the Langmuir adsorption isotherm to find maximum adsorption q_m. The unit of q is mg/g, that is, mg of heavy metal per gram of the adsorbent. All the experiments were done in triplicate and standard deviations are shown. In case the standard deviation bars are not visible, these are smaller than the size of the data mark.

Langmuir isotherms for Pb(II), As(V), and As(III), treated with NP as well as GONH, are shown in parts (a), (b), and (c), respectively, of Figure 9. The lines are the fitted curves using eq

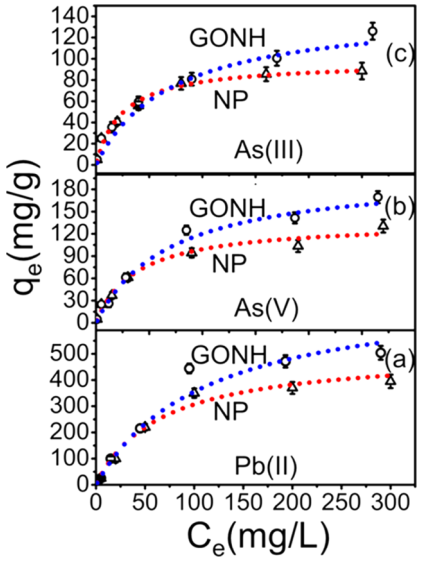

Figure 9. Langmuir adsorption isotherm for Pb(II) (a), As(V) (b), and As(III) (c) with varied initial heavy metal ion concentration ranging from 0 to 400 mg/L. pH values were kept at 5, 4, and 6.5 for Pb(II), As(V), and As(III), respectively.

1. The maximum adsorption q_m for Pb(II) using NP and GONH adsorbents was found to be 488 and 673 mg/g, respectively. The percentage removal of Pb(II) as a function of time is represented in Figure 10a. It was observed that both NP and GONH (0.02 wt %) removed 100% lead with initial concentration of 20 mg/L within 10 min. The results for As(V) are shown in Figure 9b, giving q_m = 136 mg/g for NP and q_m = 207 mg/g for GONH adsorbents. The percentage removal of As(V) with 0.02 wt % of NP and GONH is 56.5% and 58.5%, respectively (data not shown). For 0.2 wt % of NP and GONH, the percentage removal was increased to 98% and 99.5%, respectively (Figure 10b). Similarly, for As(III), q_m = 97 mg/g for NP and q_m = 146 mg/g for GONH, shown in Figure 9c. The percentage removal with 0.02 wt % of NP and GONH was

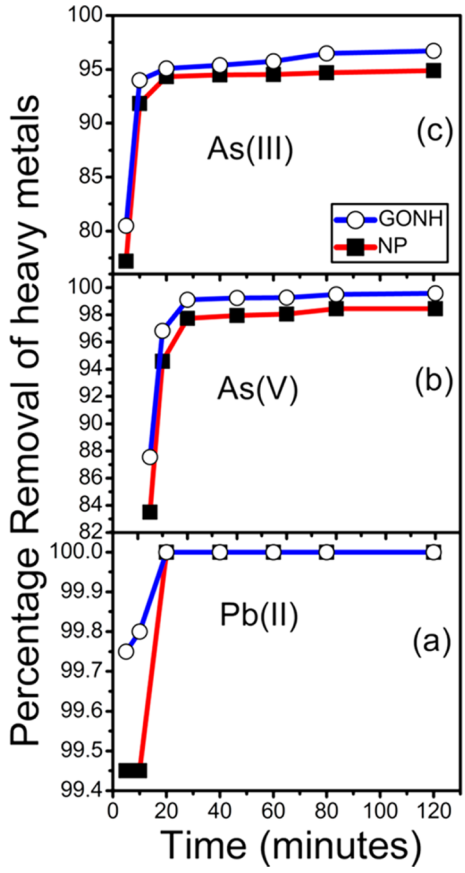

Figure 10. Kinetics of percentage removal of Pb(II) with 0.02 wt % of NP and GONH (a), As(V) with 0.2 wt % of NP and GONH (b), and As(III) with 0.2 wt % of NP and GONH (c) as a function of time with initial heavy metal ion concentration of 20 mg/L. The pH values were kept at 5, 4, and 6.5 for Pb(II), As(V), and As(III), respectively.

~50% (data not shown) whereas with 0.2 wt % it increased to 94% and 96%, respectively (Figure 10c). With pristine GO, q_m = 305, 113, and 77 mg/g for Pb(II), As(V), and As(III), respectively (see Figure S1 in the Supporting Information). The heavy metal ion adsorption on graphene oxide was very much less as compared to GONH and NP.

3.3. Adsorption Kinetics. Adsorption kinetics can be defined using pseudo-second-order equation

$$\frac{dq_t}{dt} = k_2(q_e - q_t)^2 \quad (3)$$

where q_t is the adsorption capacity of the adsorbent at time t, q_e is the adsorption capacity at equilibrium,[31,39] and k_2 (g/mg min) is the pseudo-second-order rate constant. Integration of the above equation with limits t = 0 to t and application of boundary conditions, q_t = 0 at t = 0 gives

dx.doi.org/10.1021/am504826q | ACS Appl. Mater. Interfaces 2014, 6, 17426−17436

$$\frac{t}{q_t} = \frac{1}{k_2 q_e^{\,2}} + \frac{1}{q_e} t \tag{4}$$

The values of k_2 and q_e can be computed by plotting t/q_t versus time t. The initial adsorption rate $h_0 = k_2 q_e^{\,2}$ can be calculated and the results are shown in parts (a), (b), and (c) for Pb(II), As(V), and As(III), respectively, of Figure 11. It is clear from Figure 11 that the adsorption process follows pseudo-second-order reaction. The calculated values of various parameters are given in Table 3.

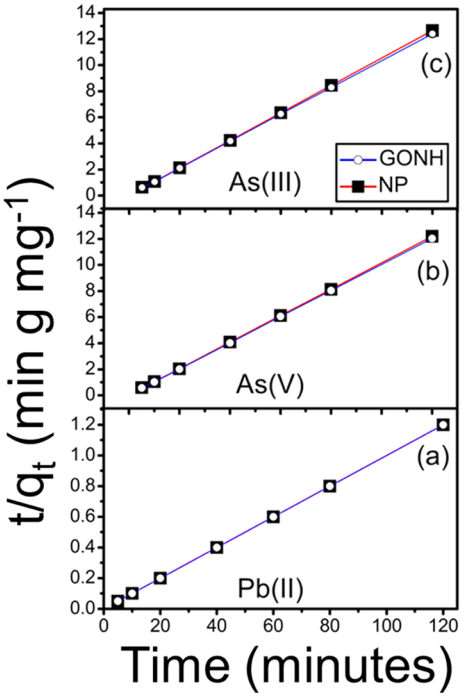

Figure 11. Pseudo-second-order kinetics graph of Pb(II) (a), As(V) (b), and As(III) (c) removal with NP and GONH.

Table 3. Adsorption Kinetics Parameters for Pb(II), As(III), and As(V)

heavy metal	adsorbent	k_2 (g mg^{-1} min^{-1})	q_e (mg g^{-1})	h_0 (mg g^{-1} min^{-1})
Pb(II) (0.02 wt %)	$MnFe_2O_4$	0.37	100	37
	GO–$MnFe_2O_4$	0.95	100	95
As(III) (0.2 wt %)	$MnFe_2O_4$	0.18	9.5	16.5
	GO–$MnFe_2O_4$	0.15	9.7	14.7
As(V) (0.2 wt %)	$MnFe_2O_4$	0.18	9.8	17.6
	GO–$MnFe_2O_4$	0.25	9.9	25

3.4. Effect of Temperature on Adsorption. To investigate the thermodynamic parameters, effect of temperature on the adsorption process was studied at three different temperatures, that is, 298, 313, and 333 K with initial concentration of heavy metal ions, 100 mg/L. The adsorption of both lead as well as arsenic was found to increase with increase in temperature. The results are shown in Figure 12. The increase in adsorption with rise in temperature is due to the increase in diffusion and decrease in viscosity of the solution.[55] Thermodynamic equilibrium constant K^0 was calculated by plotting $\ln(C_s/C_e)$ as a function of C_s (see Figure S2 in the Supporting Information). C_s is the amount of the heavy metal adsorbed per unit gram of the adsorbent (mmol/g) and C_e is the equilibrium concentration of the heavy metal ions (mmol/mL).[55] Value of Gibb's free energy can be calculated using

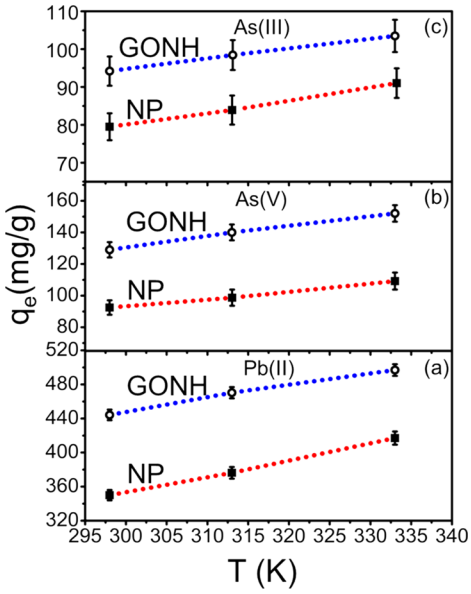

Figure 12. Heavy metal ions Pb(II) (a), As(V) (b), and As(III) (c) adsorption on GONH and NP at 298, 313, and 333 K at 100 mg/L initial concentration. pH values were kept at 5, 4, and 6.5 for Pb(II), As(V), and As(III), respectively.

$$\Delta G^\circ = -RT \ln K^\circ \tag{5}$$

where R is the universal gas constant (8.3145 J/mol·K) and T is the temperature of the solution (K).The calculated values of Gibb's free energy at different temperatures are presented in Table 4. Standard enthalpy ΔH° and ΔS° can be calculated using the van't Hoff equation:

$$\ln K^\circ = \frac{\Delta S^\circ}{R} - \frac{\Delta H^\circ}{RT} \tag{6}$$

By plotting ln K° vs $1/T$ (Figure 13), we can calculate standard entropy and standard enthalpy. The negative value of Gibb's free energy confirms that the reaction is spontaneous. When the above relations are used, the value of ΔH° is positive in each case, confirming that the reaction is endothermic.[55] The adsorption kinetics is also seen to improve with increase in temperature.

3.5. Effect of Competing Ions. Effect of competing ions is also studied by varying their concentration in heavy metal ion solution. It was observed that NO^{3-}, SO_4^{2-}, Cd^{2+}, and Zn^{2+} ions have much less effect on the adsorption capacity of GONH and NP, whereas $HCO_3^-$and HPO_4^{2-} decrease the adsorption capacity to a large extent. The effects are summarized in Tables ST1–ST6 of the Supporting Information.

3.6. Mechanisms of Adsorption. The effect of pH on anion adsorption can be understood as follows. There are a large number of –OH functional groups on oxide nanoparticles as well as on the graphene. At low pH conditions the number of H^+ ions in the solution increases and –OH groups become positively charged $-OH_2^+$, decreasing the adsorption capability of Pb(II) ions on the surface of the adsorbent. At higher pH

Table 4. Thermodynamic Parameters for Pb(II), As(V), and As(III) Adsorption on GONH and NP

heavy metal	adsorbent	temperature	% removal	K°	ΔG (kJ/mol)	ΔH (kJ/mol)
Pb(II)	GONH	298 K	100	13.72	−6.46	4.01
		313 K	100	14.80	−7.01	
		333 K	100	16.52	−7.76	
	NP	298 K	100	12.07	−6.17	5.18
		313 K	100	13.16	−6.69	
		333 K	100	15.02	−7.50	
As(V)	GONH	298 K	99.5	10.00	−5.70	6.13
		313 K	99.7	11.40	−6.32	
		333 K	99.8	13.03	−7.09	
	NP	298 K	98	9.41	−5.55	6.36
		313 K	98.3	10.60	−6.14	
		333 K	98.8	12.42	−6.95	
As(III)	GONH	298 K	96	9.37	−5.53	6.56
		313 K	96.5	10.78	−6.17	
		333 K	97	12.41	−6.95	
	NP	298 K	94	8.87	−5.40	7.25
		313 K	94.4	10.46	−6.09	
		333 K	94.8	12.13	−6.89	

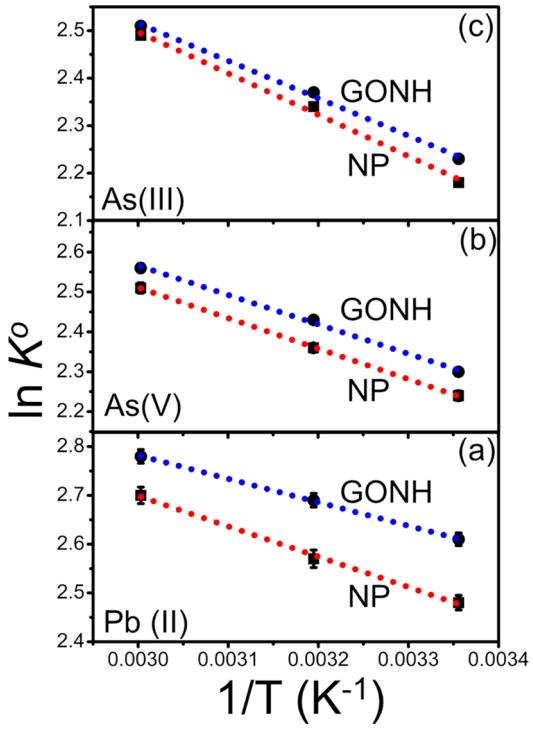

Figure 13. Variation of thermodynamic adsorption constant K° with $1/T$ for Pb(II) (a), As(V) (b), and As(III) (c) with initial concentrations 25, 50, and 100 mg/L. pH values were kept at 5, 4, and 6.5 for Pb(II), As(V), and As(III), respectively.

values −OH groups are ionized to $-O^-$, increasing the adsorption of Pb(II) ions.[51] The justification is also in accordance with surface complex formation theory.[52] This theory states that an increase in the pH decreases the competition between metal ions and protons favoring the metal ion adsorption. At pH values higher than 6, there will be a decrease in adsorption due to precipitation of Pb(II) in the form of $Pb(OH)_2$.[52] Some of the $GO-COO^-$ and $GO-O^-$ groups on the graphene may also be helping in adsorption of the lead ions through cation exchange reaction.[53] Pb(II) can be adsorbed on the surface of NP and GONH through reaction with −OH or −COOH groups on the surface of NP or GONH (at optimum pH condition):[54,55]

$$\textbf{(A)}\ M-OH+Pb^{2+} \rightarrow GO-O^{-}--Pb^{2+} + H^{+} \quad (7)$$

$$(M-OH)_2 + Pb^{2+} \rightarrow (GO-O^{-})_2--Pb^{2+} + 2H^{+} \quad (8)$$

In the above adsorption reaction M is Fe or Mn.[29] −COOH and −OH functionalities on graphene also contribute to adsorption of lead.[7]

$$\textbf{(B)}\ GO-COOH + Pb^{2+} \rightarrow GO-COO^{-}--Pb^{2+} + H^{+} \quad (9)$$

$$(GO-COOH)_2 + Pb^{2+} \rightarrow (GO-COO^{-})_2--Pb^{2+} + 2H^{+} \quad (10)$$

$$GO-OH + Pb^{2+} \rightarrow GO-O^{-}--Pb^{2+} + H^{+} \quad (11)$$

$$(GO-OH)_2 + Pb^{2+} \rightarrow (GO-O^{-})_2--Pb^{2+} + 2H^{+} \quad (12)$$

At different pH conditions, As(V) exists in different ionic and neutral forms, for example, $H_3AsO_4^0$ (pH < 2.1), $H_2AsO_4^-$ (2.1 < pH < 6.9), $HAsO_4^{2-}$ (6.9 < pH < 11.5), and AsO_4^{3-} (pH > 11.5).[56] In natural environmental pH (4−8) conditions, As(III) exists in $As(OH)_3^0$ and $AsO(OH)_2^-$ and As(V) exists in $H_2AsO_4^-$ and $HAsO_4^{2-}$ ionic forms.[57] In pH range < 4.3, the concentration of $H_2AsO_4^-$ is higher and −OH groups on nanoparticles become $-OH_2^+$, favoring the adsorption of As(V).[58] On the other hand, As(III) is converted into As(V) in the presence of manganese oxide. Oxidation of As(III) to As(V) in Mn environment creates a greater number of active sites for the adsorption process. Manganese(II) arsenate, $Mn_3(AsO_4)_2$, is also precipitated in the reaction, causing the decrease in the pH of the solution, favoring the adsorption process.[59] Also due to the presence of iron oxide, a complex, $>FeOH_2^+\_AsO(OH)_2^-$, is also formed due to reaction with As(III).[60] The abundant −OH groups may also be helping the adsorption process in a similar manner. Arsenic can react with GONH or NP adsorbent at optimum pH conditions as follows:[61,29]

dx.doi.org/10.1021/am504826q | ACS Appl. Mater. Interfaces 2014, 6, 17426−17436

$$\textbf{(C)}\ M{-}OH_2^+ + H_2AsO_4^- \rightarrow M{-}OH_2^+{-}{-}H_2AsO_4^- \quad (13)$$

$$(M{-}OH_2^+)_2 + HAsO_4^{2-} \rightarrow (M{-}OH_2^+)_2{-}{-}HAsO_4^- \quad (14)$$

$$M{-}OH + HAsO_2 \rightarrow M{-}OH \leftarrow HAsO_2 \quad (15)$$

$$\textbf{(D)}\ GO{-}COOH_2^+ + H_2AsO_4^- \rightarrow GO{-}COOH_2^+{-}{-}H_2AsO_4^- \quad (16)$$

$$(GO{-}COOH_2^+)_2 + HAsO_4^{2-} \rightarrow (GO{-}COOH_2^+)_2{-}{-}HAsO_4^- \quad (17)$$

$$GO{-}COOH + HAsO_2 \rightarrow GO{-}COOH \leftarrow HAsO_2 \quad (18)$$

$$\textbf{(E)}\ GO{-}OH_2^+ + H_2AsO_4^- \rightarrow GO{-}COOH_2^+{-}{-}H_2AsO_4^- \quad (19)$$

$$(GO{-}OH_2^+)_2 + HAsO_4^{2-} \rightarrow (GO{-}COOH_2^+)_2{-}{-}HAsO_4^- \quad (20)$$

$$GO{-}OH + HAsO_2 \rightarrow GO{-}COOH \leftarrow HAsO_2 \quad (21)$$

3.7. Desorption Studies. During desorption study, 99% of adsorbed As(V) was released from both the GONH and NP adsorbents by treatment with 1 M NaOH. These results are consistent with the previous report.[31] In the case of As(III), desorption percentage was found to be 93% and 90% for GONH and NP adsorbents, respectively. At high pH values, the surface −OH and −COOH groups undergo deprotonation and become negatively charged, leading to desorption of the negatively charged arsenic ions. There was no considerable variation in adsorption and desorption values until five cycles.

Desorption studies for Pb(II) was studied using 0.2 M HCl. At low pH conditions the surface −OH and −COOH groups become more protonated, becoming positively charged and hence leading to desorption of the positively charged ions. In this case GONH as well as NP adsorbents desorbed ∼99% of the adsorbed Pb(II). There is no considerable change in adsorption and desorption efficiencies, even after five cycles. These results show that both GONH and NP are very good adsorbents with high adsorption and desorption capabilities under different pH conditions. The results also affirm the regeneration and reusability of these adsorbents by following a simple desorption process.

4. CONCLUSIONS

Table 1 compares the adsorption capacities of different adsorbents for heavy metals Pb(II), As(III), and As(V) known so far in the literature with our present study on GO−$MnFe_2O_4$ nanohybrids and the reference $MnFe_2O_4$ nanoparticles. It is clear that the adsorption capacity of GO−$MnFe_2O_4$ nanohybrids is superior to all the adsorbents reported so far for the removal of Pb(II), As(III), and As(V). This exceptional adsorption property is due to the combination of the unique layered nature (allowing maximum surface area) of the hybrid system and the good adsorption capabilities of both the GO and NP. Needless to emphasize, an easy magnetic separation of the GONH hybrids and rapid adsorption rates make this material very attractive for use in water treatment. The use of GONH in water treatment can be done by directly adding the adsorbent and subsequently removing it magnetically, by making a membrane or by coating it on ceramic beads or sand particles. It will be interesting to explore graphene oxide−nanoparticle hybrids for removal of other heavy metals and contaminants in water.

■ ASSOCIATED CONTENT

Supporting Information

Tables showing effect of competing ions on the adsorption of Pb(II), As(III), and As(V) on NP and GONH; Langmuir isotherm of adsorption of Pb(II), As(III), and As(V) on GO; ln C_s/C_e vs C_s plot. This material is available free of charge via the Internet at http://pubs.acs.org.

■ AUTHOR INFORMATION

Corresponding Author

*E-mail: asood@physics.iisc.ernet.in.

Notes

The authors declare no competing financial interest.

■ ACKNOWLEDGMENTS

A.K.S. thanks the Department of Science and Technology for support under Nanomission. S.K. thanks University Grants Commission for Dr. D. S. Kothari Fellowship.

■ REFERENCES

(1) Henke, K. *Arsenic: Environmental Chemistry, Health Threats, and Waste Treatment*, 1st ed; Wiley: West Sussex, 2009.
(2) Nickson, R.; McArthur, J.; Burgess, W.; Ahmed, K. M.; Ravenscroft, P.; Rahman, M. A. Arsenic Poisoning of Bangladesh Groundwater. *Nature* **1998**, *395*, 338.
(3) Mishra, A. K.; Ramaprabhu, S. Functionalized Graphene Sheets for Arsenic Removal and Desalination of Sea Water. *Desalination* **2011**, *282*, 39−45.
(4) Nordstrom, D. K. Worldwide Occurrences of Arsenic in Ground Water. *Science* **2002**, *296*, 2143−2144.
(5) Zhang, K.; Dwivedi, V.; Chi, C.; Wu, J. Graphene Oxide/Ferric Hydroxide Composites for Efficient Removal of As in Drinking Water. *J. Hazard. Mater.* **2010**, *182*, 162−168.
(6) Dey, T. In *Nanotechnology for Water Purification*; BrownWalker Press: Boca Raton, FL, 2012; Chapter 1, pp 1−29.
(7) Madadrang, C. J.; Kim, H. Y.; Gao, G.; Wang, N.; Zhu, J.; Feng, H.; Gorring, M.; Kasner, M. L.; Hou, S. Adsorption Behavior of EDTA-Graphene Oxide for Pb(II) Removal. *ACS Appl. Mater. Interfaces* **2012**, *4*, 1186−1193.
(8) Ali, I. New Generation Adsorbents for Water Treatment. *Chem. Rev.* **2012**, *112*, 5073−5091.
(9) Yavuz, C. T.; Mayo, J. T.; Yu, W. W.; Prakash, A.; Falkner, J. C.; Yean, S.; Cong, L.; Shipley, H. J.; Kan, A.; Tomson, M.; Natelson, D.; Colvin, V. L. Low-Field Magnetic Separation of Monodisperse Fe_3O_4Nanocrystals. *Science* **2006**, *314*, 964−967.
(10) Lu, A. H.; Salabas, E. L.; Schüth, F. Magnetic Nanoparticles: Synthesis, Protection, Functionalization, and Application. *Angew. Chem., Int. Ed.* **2007**, *46*, 1222−1244.
(11) Zhang, W. Nanoscale Iron Particles for Environmental Remediation: An Overview. *J. Nanopart. Res.* **2003**, *5*, 323−332.
(12) Rajeswar, K.; Chenthamarakshun, C. R.; Goeringer, S.; Djukic, M. Materials, Mechanistic Issues and Implications for Environmental Remediation. *Pure Appl. Chem.* **2001**, *73*, 1849−1860.
(13) Bowman, R. S. Applications of Surfactant-Modified Zeolites to Environmental Remediation. *Microporous Mesoporous Mater.* **2002**, *61*, 43−56.
(14) Kamat, P. V.; Huehn, R.; Nicolaescu, R. A Sense and Shoot Approach for Photocatalytic Degradation of Organic Contaminants in Water. *J. Phys. Chem. B* **2002**, *106*, 788−794.

(15) Goel, J.; Kadirvelu, K.; Rajagopal, C.; Garg, V. K. Removal of Lead (II) from Aqueous Solution by Adsorption on Carbon Aerogel Using a Response Surface Methodological Approach. *Ind. Eng. Chem. Res.* **2005**, *44*, 1987−1994.
(16) Al-Degs, Y.; Khraisheh, M. A. M.; Tutunji, M. F. Sorption of Lead Ions on Diatomite and Manganese Oxides Modified Diatomite. *Water Res.* **2001**, *35*, 3724−3728.
(17) Malika, D. J.; Strelko, V.; Streata, M.; Puziy, A. M. Characterisation of Novel Modified Active Carbons and Marine Algal Biomass for the Selective Adsorption of Lead. *Water Res.* **2002**, *36*, 1527−1538.
(18) Pan, B. C.; Pan, B. J.; Chen, X. Q.; Zhang, W. M.; Zhang, Q. J.; Zhang, Q. X.; Chen, J. L. Preparation and Preliminary Assessment of Polymer-Supported Zirconium Phosphate for Selective Lead Removal from Contaminated Water. *Water Res.* **2006**, *40*, 2938−2946.
(19) Nelson, Y. M.; Lion, L. W.; Shuler, M. L.; Ghiorse, W. C. Lead Adsorption to Mixtures of Biogenic Mn Oxides and Fe Oxides. *Environ. Sci. Technol.* **2002**, *36*, 421−425.
(20) Driehaus, W.; Seith, R.; Jekel, M. Oxidation of Arsenate (III) with Manganese Oxides in Water Treatment. *Water Res.* **1995**, *29*, 297−305.
(21) Bajpai, S.; Chaudhuri, M. Removal of Arsenic from Ground Water by Manganese Dioxide−Coated Sand. *J. Environ. Eng.* **1999**, *8*, 782−784.
(22) Chiu, V. Q.; Hering, J. G. Arsenic Adsorption and Oxidation at Manganite Surfaces. 1. Method for Simultaneous Determination of Adsorbed and Dissolved Arsenic Species. *Environ. Sci. Technol.* **2000**, *34*, 2029−2034.
(23) Tournassat, C.; Charlet, L.; Bosbach, D.; Manceau, A. Arsenic(III) Oxidation by Birnessite and Precipitation of Manganese-(II) Arsenate. *Environ. Sci. Technol.* **2002**, *36*, 493−500.
(24) Manning, B. A.; Fendorf, S. E.; Bostick, B.; Suarez, D. L. Arsenic(III) oxidation and Arsenic(V) Adsorption Reactions on Synthetic Birnessite. *Environ. Sci. Technol.* **2002**, *36*, 976−981.
(25) Oscarson, D. W.; Huang, P. M.; Defosse, C.; Herbillon, A. Oxidative Power of Mn (IV) and Fe (III) Oxides with Respect to As (III) in Terrestrial and Aquatic Environments. *Nature* **1981**, *291*, 50−51.
(26) Yean, S.; Cong, L.; Yavuz, C. T.; Mayo, J. T.; Yu, W. W.; Kan, A. T.; Colvin, V. L.; Tomson, M. B. Effect of Magnetite Particle Size on Adsorption and Desorption of Arsenite and Arsenate. *J. Mater. Res.* **2005**, *20*, 3255−3264.
(27) Deschamps, E.; Ciminelli, V. S. T.; Höll, W. H. Removal of As (III) and As (V) from Water Using a Natural Fe and Mn Enriched Sample. *Water Res.* **2005**, *39*, 5212−5220.
(28) Zhang, G.; Qu, J.; Liu, H.; Liu, R.; Wu, R. Preparation and Evaluation of a Novel Fe-Mn Binary Oxide Adsorbent for Effective Arsenite Removal. *Water Res.* **2007**, *41*, 1921−1928.
(29) Hu, J.; Lo, L. M.C.; Chen, G. Fast Removal and Recovery of Cr (VI) Using Surface-Modified Jacobsite ($MnFe_2O_4$) Nanoparticles. *Langmuir* **2005**, *21*, 11173−11179.
(30) Wu, R.; Qu, J. Removal of Water-Soluble Azo Dye by the Magnetic Material $MnFe_2O_4$. *J. Chem. Technol. Biotechnol.* **2005**, *80*, 20−27.
(31) Zhang, S.; Niu, H.; Cai, Y.; Zhao, X.; Shi, Y. Arsenite and Arsenate Adsorption on Coprecipitated Bimetal Oxide Magnetic Nanomaterials: $MnFe_2O_4$ and $CoFe_2O_4$. *Chem. Eng. J.* **2010**, *158*, 599−607.
(32) Yang, S. T.; Chang, Y. L.; Wang, H. F.; Liu, G. B.; Chen, S.; Wang, Y. W.; Liu, Y. F.; Cao, A. N. Folding/Aggregation of Graphene Oxide and its Application in Cu^{2+} Removal. *J. Colloid Interface Sci.* **2010**, *351*, 122−127.
(33) Wang, S.; Sun, H.; Ang, H. M.; Tade, M. O. Adsorptive Remediation of Environmental Pollutants Using Novel Graphene-based Nanomaterials. *Chem. Eng. J.* **2013**, *226*, 336−347.
(34) Yang, X.; Zhang, X.; Ma, Y.; Huang, Y.; Wang, Y.; Chen, Y. Superparamagnetic Graphene Oxide − Fe_3O_4 Nanoparticles Hybrid for Controlled Targeted Drug Carriers. *J. Mater. Chem.* **2009**, *19*, 2710−2714.
(35) Chung, C.; Kim, Y. K.; Shin, D.; Ryoo, S. R.; Hong, B. H.; Min, D. H. Biomedical Applications of Graphene and Graphene Oxide. *Acc. Chem. Res.* **2013**, *46*, 2211−2224.
(36) Marcano, D. C.; Kosynkin, D. V.; Berlin, J. M.; Sinitskii, A.; Sun, Z.; Slesarev, A.; Alemany, L. B.; Lu, W.; Tour, J. M. Improved Synthesis of Graphene Oxide. *ACS Nano* **2010**, *4*, 4806−4814.
(37) Huang, N. M.; Lim, H. N.; Chia, C. H.; Yarmo, M. A.; Muhamad, M. R. Simple Room-Temperature Preparation of High-Yield Large-Area Graphene Oxide. *Int. J. Nanomed.* **2011**, *6*, 3443−3448.
(38) Sood, A. K.; Chakraborty, B. In *Graphene: Synthesis, Properties and Applications*; Rao, C. N. R., Sood, A. K., Eds.; Wiley-VCH Verlag GMbH & Co. KGaA: Weinheim, Germany, 2013; Chapter 2, pp 49−87.
(39) Chandra, V.; Park, J.; Chun, Y.; Lee, J. W.; Hwang, I. C.; Kim, K. S. Water-Dispersible Magnetite-Reduced Graphene Oxide Composites for Arsenic Removal. *ACS Nano* **2010**, *4*, 3979−3986.
(40) Sim, L. C.; Leong, K. H.; Ibrahima, S.; Saravanan, P. Graphene Oxide and Ag Engulfed TiO_2 Nanotube Arrays for Enhanced Electron Mobility and Visible-Light-Driven Photocatalytic Performance. *J. Mater. Chem. A* **2014**, *2*, 5315−5322.
(41) Upadhyay, R. V.; Davies, K. J.; Wells, S.; Charles, S. W. Preparation and Characterization of Ultra-Fine $MnFe_2O_4$ and $Mn_xFe_{1-x}Fe_2O_4$ Spinel Systems: I. Particles. *J. Magn. Magn. Mater.* **1994**, *132*, 249−257.
(42) Xiao, Y.; Zai, J.; Tao, L.; Li, B.; Han, Q.; Yu, C.; Qian, X. $MnFe_2O_4$−Graphene Nanocomposites with Enhanced Performances as Anode Materials for Li-ion Batteries. *Phys. Chem. Chem. Phys.* **2013**, *15*, 3939−3945.
(43) Ma, Z.; Zhao, D.; Chang, Y.; Xing, S.; Wua, Y.; Gao, Y. Synthesis of $MnFe_2O_4$@Mn−Co Oxide Core−Shell Nanoparticles and Their Excellent Performance for Heavy Metal Removal. *Dalton Trans.* **2013**, *42*, 14261−14267.
(44) Bellusci, M.; Aliotta, C.; Fiorani, D.; Barbera, A. L.; Padella, F.; Peddis, D.; Pilloni, M.; Secci, D. Manganese Iron Oxide Superparamagnetic Powder by Mechanochemical Processing: Nanoparticles Functionalization and Dispersion in a Nanofluid. *J. Nanopart. Res.* **2012**, *14*, 1−11.
(45) Guo, J.; Wang, R.; Tiju, W. W.; Pan, J.; Liua, T. Synthesis of Fe Nanoparticles@Graphene Composites for Environmental Applications. *J. Hazard. Mater.* **2012**, *225*, 63−67.
(46) Islam, M. R.; Joung, D.; Khondaker, S. I. Schottkey Diode via Electrophoretic Assembly of Reduced Graphene Oxide Sheets Between Dissimilar Metal Electrodes. *New J. Phys.* **2011**, *13*, 035021.
(47) Nesbitt, H. W.; Canning, G. W.; Bancroft, G. M. XPS Study of Reductive Dissolution of 7Å-Birnessite by H_3AsO_3, with Constraints on Mechanism. *Geochim. Cosmochim. Acta* **1998**, *62*, 2097−2110.
(48) Manning, T. J.; William, R. Inductively Coupled Plasma - Atomic Emission Spectrometry. *Chem. Educ.* **1997**, 1−19.
(49) Issabayeva, G.; Aroua, M. K. Removal of Copper and Zinc Ions onto Biomodified Palm Shell Activated Carbon. *Int. J. Chem. Nucl. Metall. Mater. Eng.* **2011**, *5*, 26−29.
(50) McBridge, M. B. A Critique of Diffuse Double Layer Models Applied to Colloid and Surface Chemistry. *Clays Clay Miner.* **1997**, *45*, 598−608.
(51) Hoa, Y. S.; Ofomaja, A. E. Pseudo-Second-Order Model for Lead Ion Sorption from Aqueous Solutions onto Palm Kernel Fiber. *J. Hazard. Mater.* **2006**, *B129*, 137−142.
(52) Kosa, S. A.; Zhrani, G. A.; Salam, M. A. Removal of Heavy Metals from Aqueous Solutions by Multi-Walled Carbon Nanotubes Modified with 8-Hydroxyquinoline. *Chem. Eng. J.* **2012**, *181−182*, 159−168.
(53) Li, Y. H.; Ding, J.; Luan, Z.; Di, Z.; Zhu, Y.; Xu, C.; Wu, D.; Wei, B. Competitive Adsorption of Pb^{2+}, Cu^{2+} and Cd^{2+} Ions from Aqueous Solutions by Multiwalled Carbon Nanotubes. *Carbon* **2003**, *41*, 2787−2792.
(54) Ren, Y.; Li, N.; Feng, J.; Luan, T.; Wen, Q.; Li, Z.; Zhang, M. Adsorption of Pb(II) and Cu(II) from Aqueous Solution on Magnetic

Porous Ferrospinel $MnFe_2O_4$. *J. Colloid Interface Sci.* **2012**, *367*, 415−421.
(55) Yu, X. Y.; Luo, T.; Zhang, Y. X.; Jia, Y.; Zhu, B. J.; Fu, X. C.; Liu, J. H.; Huang, X. J. Adsorption of Lead (II) on O_2-Plasma-Oxidized Multiwalled Carbon Nanotubes: Thermodynamics, Kinetics, and Desorption. *ACS Appl. Mater. Interfaces* **2011**, *3*, 2585−2593.
(56) Tuutijarvi, T.; Lu, J.; Sillanpaa, M.; Chen, G. Adsorption Mechanism of Arsenate on Crystal γ-Fe_2O_3 Nanoparticles. *J. Environ. Eng.* **2010**, *136*, 897−905.
(57) Sharma, V. K.; Sohn, M. Aquatic Arsenic: Toxicity, Speciation, Transformations, and Remediation. *Environ. Int.* **2009**, *35*, 743−759.
(58) Sheng, G.; Li, Y.; Yang, X.; Ren, X.; Yang, S.; Hu, J.; Wang, X. Efficient Removal of Arsenate by Versatile Magnetic Graphene Oxide Composites. *RSC Adv.* **2012**, *2*, 12400−12407.
(59) Lenoble, V.; Laclature, C.; Serpaud, B.; Deluchat, V.; Bollinger, J. C. As (V) Retention and As (III) Simultaneous Oxidation and Removal on a MnO_2 -Loaded Polystyrene Resin. *Sci. Total Environ.* **2004**, *326*, 197−207.
(60) Sverjensky, D. A.; Fukushi, K. A Predictive Model (ETLM) for As (III) Adsorption and Surface Speciation on Oxides Consistent with Spectroscopic Data. *Geochim. Cosmochim. Acta* **2006**, *70*, 3778−3802.
(61) Sarkar, S.; Blaney, L. M.; Gupta, A.; Ghosh, D.; Sengupta, A. K. Arsenic Removal from Ground Water and its Safe Containment in a Rural Environment: Validation of a Sustainable Approach. *Environ. Sci. Technol.* **2008**, *42*, 4268−4273.
(62) Fan, L.; Luo, C.; Sun, M.; Li, X.; Qiu, H. Highly Selective Adsorption of Lead Ions by Water-dispersible Magnetic Chitosan/Graphene Oxide Composites. *Colloids Surf., B* **2013**, *103*, 523−529.
(63) Vukovic, G. D.; Marinkovic, A. D.; Skapin, S. D.; Ristic, M. D.; Aleksic, R.; Peric-Grujic, A. A.; Uskokovic, P. S. Removal of Lead from Water by Amino Modified Multi-Walled Carbon Nanotubes. *Chem. Eng. J.* **2011**, *173*, 855−865.
(64) Ngah, W. S. W.; Fatinathan, S. Pb (II) Biosorption Using Chitosan and Chitosan Derivatives Beads: Equilibrium, Ion Exchange and Mechanism Studies. *J. Environ. Sci.* **2010**, *22*, 338−346.
(65) Huang, Z.; Zheng, X.; Lv, W.; Wang, M.; Yang, Q.; Kang, F. Adsorption of Lead (II) Ions from Aqueous Solution on Low-Temperature Exfoliated Graphene Nanosheets. *Langmuir* **2011**, *27*, 7558−7562.
(66) Mishra, A. K.; Ramaprabhu, S. The Role of Functionalised Multiwalled Carbon Nanotubes Based Supercapacitor for Arsenic Removal and Desalination of Sea Water. *J. Exp. Nanosci.* **2012**, *7*, 85−97.
(67) Mishra, A. K.; Ramaprabhu, S. Magnetite Decorated Multiwalled Carbon Nanotube Based Supercapacitor for Arsenic Removal and Desalination of Seawater. *J. Phys. Chem. C* **2010**, *114*, 2583−2590.
(68) Zhao, G.; Ren, X.; Gao, X.; Tan, X.; Li, J.; Chen, C.; Huang, Y.; Wang, X. Removal of Pb(II) Ions from Aqueous Solutions on Few-Layered Graphene Oxide Nanosheets. *Dalton Trans.* **2011**, *40*, 10945−10952.
(69) He, Y. Q.; Zhang, N. N.; Wang, X. D. Adsorption of Graphene Oxide/Chitosan Porous Materials for Metal Ions. *Chin. Chem. Lett.* **2011**, *22*, 859−862.
(70) Zhang, N.; Qiu, H.; Si, Y.; Wang, W.; Gao, J. Fabrication of Highly Porous Biodegradable Monoliths Strengthened by Graphene Oxide and their Adsorption of Metal Ions. *Carbon* **2011**, *49*, 827−837.